Journal of Photochemistry & Photobiology, A: Chemistry 418 (2021) 113375

Contents lists available at ScienceDirect

Journal of Photochemistry & Photobiology, A: Chemistry

journal homepage: www.elsevier.com/locate/jphotochem

New photochromic azoderivatives with potent acetylcholinesterase inhibition

Brunella Biscussi [a,1,*], Maria Alejandra Sequeira [a,1], Victoria Richmond [b], Pau Arroyo Mañez [b], Ana Paula Murray [a]

[a] INQUISUR-CONICET, Departamento de Química, Universidad Nacional del Sur, Bahía Blanca, Argentina
[b] UMYMFOR (CONICET-UBA), Departamento de Química Orgánica, Facultad de Ciencias Exactas y Naturales, Universidad de Buenos Aires, Ciudad Universitaria, Buenos Aires, Argentina

ARTICLE INFO

Keywords:
Photochromic compounds
Acetylcholinesterase inhibition
Alzheimer's disease
Azoderivatives
Microwave assisted synthesis

ABSTRACT

The design of photochromic cholinesterase inhibitors is a challenge of the photopharmacological approach towards the remote control of acetylcholinesterase (AChE) enzyme and its potential application in Alzheimer's disease therapy. In this work, a series of azoderivatives were designed, synthesized and evaluated as AChE inhibitors. The optimized microwave-assisted synthesis (two steps) showed excellent yields with a total reaction time no longer than 40 min. The results showed that all the synthesized compounds exhibited high AChE inhibitory activity at the micromolar range (IC_{50}, 0.65–8.52 μM). Moreover, compound 19, with double four-hydrocarbon chain connected to piperidine, showed a powerful *in vitro* enzymatic response for its *Z* isomer (IC_{50}: 0.43 μM) determined by Ellman's assay. Also, 19 showed a stable photostationary state monitored by UV/Vis absorption spectroscopy and ^{1}H NMR spectra. These results indicate that 19 can act as an efficient photoresponsible probe to remote control AChE activity. Molecular modelling analysis of 19 *Z* revealed its affinity by the peripheral anionic site of AChE, providing understanding of its higher inhibition power. This study contributes to the development of new promising agents for photopharmacological treatment of Alzheimer's disease.

1. Introduction

Alzheimer's disease (AD) is the principal cause of dementia among people over 65 years old. It is a progressive disease, in which the symptoms of dementia gradually get worse over the years. AD affects memory, thinking, reasoning and language skills, developing changes in the patient's personality leaving him unable to care for himself. Neuropathologically, AD is characterized by extracellular deposits of a beta-amyloid peptide (Aβ), called senile plaques or amyloid plaques, intracellular deposits of hyperphosphorylated tau protein known as neurofibrillary tangles or NFTs, neuronal loss and synaptic loss [1–3]. Cholinesterase inhibitors play an important role in enhancing synaptic cholinergic activity, and consequently, have therapeutic application related to AD, myasthenia gravis, and glaucoma [4]. The main therapeutic approach for AD, based on the so-called "cholinergic hypothesis", is the treatment with acetylcholinesterase inhibitors (AChEI). This kind of drugs improves the cognitive function by enhancing the levels of the neurotransmitter acetylcholine by the inhibition of the enzyme responsible for its degradation, AChE (E.C. 3.1.1.7). Nowadays, there are five approved drugs to treat AD patients: tacrine (already withdrawn from the market due to its hepatotoxicity); donepezil; rivastigmine and galantamine, all of them AChEI; and memantine, an N-methyl--D-aspartate receptor (NMDA) antagonist [2,5,6]. Unfortunately, even if these drugs are useful in improving AD patient's life quality, they are unable to stop or alter the outcome of the disease. Therefore, finding new agents to treat AD is a goal of utmost importance for the scientific community.

AChE has a catalytic active site (CAS), constituted by a catalytic triad located at the bottom of the gorge at 20 Å from the entrance, where the hydrolysis of neurotransmitter takes place [7]. AChE also features a "peripheral anionic site" (PAS) related to the modulation of the catalytic activity, which is located at the entrance of the gorge. The PAS has been reported to be involved in the pro-aggregating action of AChE toward β-amyloid peptide, an important factor in the onset and progression of

* Corresponding author.
E-mail address: brunella.biscussi@uns.edu.ar (B. Biscussi).
[1] These authors contributed equally to the work.

https://doi.org/10.1016/j.jphotochem.2021.113375
Received 20 January 2021; Received in revised form 13 April 2021; Accepted 18 May 2021
Available online 24 May 2021

AD [8]. Elucidating AChEI's ability to simultaneously interact with catalytic and peripheral binding sites has thus become an incipient research area [9].

Lately, the idea of photopharmacology based on the use of synthetic photoswitches to control biological activity has become an important research field with a promising future in medicine and biology applications [10,11].

In this context, there is an increasing interest in the design of photochromic AChEI, looking forward to achieve AChE photocontrol. A recent example of this kind of AChEI is the work published by Trauner et al., in which enzymatic photocontrol was observed in a series of tacrine-azobencene hybrids [12]. The "azologization" (azobenzene + analogization) strategy, propose that azobenzene can mimic structural motifs ("azosteres") found in drugs or drug candidates such as stilbenes, (heterocyclic) N-aryl benzamides, benzyl phenyl (thio)ethers, benzyl anilines, and 1,2- diaryl ethanes, with the advantage that the azobenzene nucleus offers the possibility for light sensitization and light-dependent control of its functions [13–15]. Recently, our group has reported the synthesis of a series of aza-stilbene analogs with potent AChE inhibition [16]. Molecular modelling of these compounds showed a dual interaction with both the PAS and the CAS of the enzyme [16]. Keeping in mind these results and inspiring ourselves in the "azologization" concept, we rationally designed a small library of new compound replacing the aza-stilbene (Ph-C = N-Ph) scaffold by an azobenzene (Ph-N = N-Ph) structure, looking forward to develop new photomodulable AChEIs with potent enzyme inhibition [16] (Fig. 1).

In this work, we present the microwave-assisted synthesis and structural characterization of new azoderivatives with potential application as reversible photochromic AChEI, which showed *in vitro* enzymatic response for both (*E*) and (*Z*) isomers. AChE activity was determined by Ellman's assay in the presence of the reversible photoswitchable blockers, whose *in vitro* photoisomerization efficiency was evaluated by UV/Vis absorption spectroscopy and ^{1}H NMR. The purpose of this work is to make a contribution in the field of new synthetic photomodulable drugs for the treatment of AD.

2. Results and discussion

2.1. Chemistry

Based on our previous results with aza-stilbene analogs that exhibited dual AChE inhibition, and hoping to obtain azoderivatives with potential application as reversible photochromic AChEI, we decided to exchange the aza-stilbene structure (Ph-C = N-Ph) by a photomodulable azobenzene core (Ph-N = N-Ph), preserving the linker successfully designed to allow interaction with both target sites, CAS and PAS of the enzyme.

The monosubstituted derivatives 6–11 were synthesized from (*E*)-4-(phenyldiazenyl)phenol (1) by two consecutive reactions: first with the corresponding dibromoalkane and subsequently with a secondary amine (pyrrolidine, piperidine and piperazine) (Scheme 1). These two synthetic steps were carried out using the optimized microwave heating method, showing great yield advantages and reducing purifications stages over the conventional method of prolonged heating.

The preparation of the disubstituted azobenzene derivatives 17−24 was carried out using the procedures shown in Scheme 2. The first synthetic step was conducted in a conventional manner, following a known procedure [17]. Then, azoderivatives were prepared in high yields and in shorter reaction times using the optimized microwave heating method.

The design of the azobenzene derivatives with a doble substitution in positions 4 and 4′ was inspired in the evidence that substituents bearing electron donor groups promote an efficient photoisomerization of the azobenzene with a slow thermal back *Z-E* isomerization. Upon isomerization from the *E*-form to the *Z*-form, the distance between the substituents in 4 and 4′ positions varies from 9.0 Å for *E* isomer to 5.5 Å in *Z* isomer (Fig. 2a).

This remarkably large change (the *E*-azobenzene molecule itself is 9 Å long) could be amplified with appropriate substitution. Furthermore, *E* azobenzene possess a zero dipolar moment, while *Z* isomers display an increase of around 4 D in many cases [18].

The purpose of this work was to study and understand how enzyme-inhibitor interaction is influenced by characteristics such as mono- and disubstitution, linker length, and *Z/E* configuration.

2.2. In vitro inhibition studies on AChE

The enzymatic inhibition against AChE was evaluated for compounds 6–11 and 17−24 by the Ellman's spectrophotometric method with slight modifications [19]. Tacrine, a known cholinesterase inhibitor was included as reference compound. The inhibitor concentration necessary to reduce the enzyme activity to a 50 % (IC_{50}) for all the analogs is summarized in Table 1. The results show that most of the tested compound, except 11, can inhibit the AChE, showing moderate to potent inhibition.

These results show a structure-activity relationship which follows a tendency respect to the length of the compound's linker, as occurred with the aza-stilbene derivatives previously studied in our group [16]. Concerning monosubstituted azobenzene derivatives, the most potent inhibitor was 8 (IC_{50} = 0.95 μM), with a seven-carbon chain connected to piperidine. On the other hand, compound 21 (IC_{50} = 0.65 μM), with double five-carbon chains connected to piperidine, was the most active of the disubstituted azobenzene series, while 19 and 22 exhibited also low IC_{50} values, under 1 μM, behaving as potent AChE inhibitors. All these results demonstrate increased activity for piperidine substituted compounds compared to pyrrolidine substituted ones, for the same linker length.

Compound 11, with seven-methylene chain connected to piperazine, was the only one in the series that did not show inhibitory activity against AChE. The only difference between 11 and 8 (IC_{50} = 0.96 μM) is

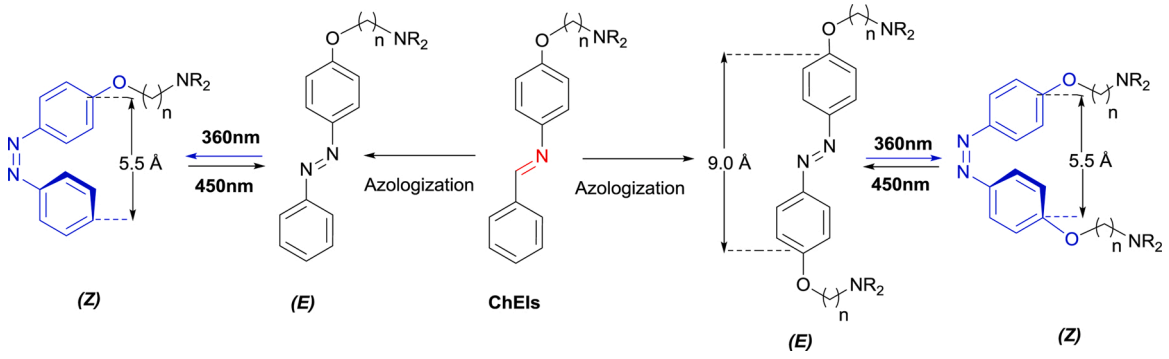

Fig. 1. Application of the azologization principle to aza-stilbene derivatives, reported as dual ChEIs.

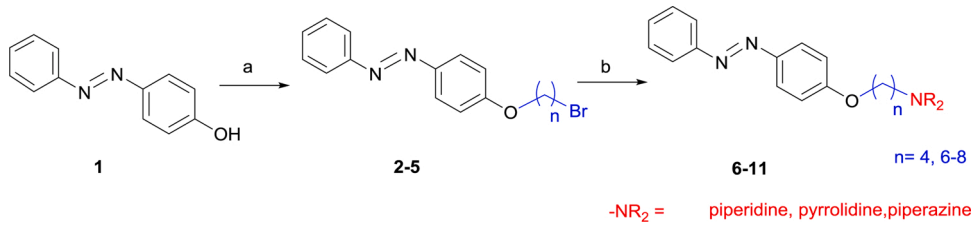

Scheme 1. Synthetic pathway of monosubstituted azobenzene derivatives. (a) $Br(CH_2)_nBr$, K_2CO_3, CH_3CN, MW 10′. (b) NHR_2, DMF, MW 8-10′.

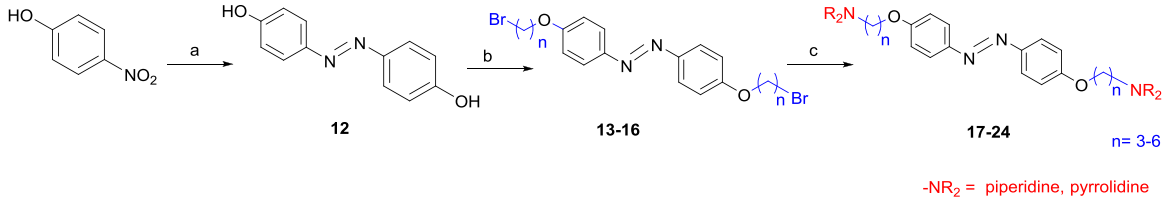

Scheme 2. Synthetic pathway of disubstituted azobenzene derivatives. (a) KOH/H_2O, 120 °C, 1 h. (b) $Br(CH_2)_nBr$, K_2CO_3, CH_3CN, MW 20′. (b) NHR_2, K_2CO_3, DMF, MW 20′.

the presence of N-H in position 4 of the piperazine ring. This result may be attributed to the electron withdrawing effect of the second nitrogen atom, which could reduce the electron density of the tertiary amine, affecting its protonation and thus reducing the interaction between ammonium and the catalytic active site of AChE. A similar effect was observed for flavonoids and diterpenoids linked to cyclic amines possessing an additional nitrogen or oxygen atom in the terminal group [20, 21].

2.3. *E-Z photoisomerization detected by UV–vis spectroscopy and ^1H NMR spectroscopy*

In order to evaluate the photomodulation ability of these compounds, two monosubstituted (7 and 9) and two disubstituted (17 and 19) azobenzene derivatives were selected for further study. The choice was made based on their different linker length and their remarkable differences in their IC_{50} values. The photomodulation ability of compounds 7, 9, 17 and 19 was evaluated through UV–vis spectroscopy experiments. In methanol, the yellowish solution of 7 *(E)*, 9 *(E)*, 17 *(E)* and 19 *(E)* changed to orange upon UV-light illumination (360 nm, 8 W, 5 min) when the stabilized photostationary state (pss) of *E:Z* was reached (named 7 *(Z)*, 9 *(Z)*, 17 *(Z)* and 19 *(Z)*) (Table 2).

The photoconversion from *E* to *Z* isomer was also studied by UV − Vis spectroscopy. E:Z ratios are reported in Table 2, for compounds 7, 9, 17 and 19. The UV − Vis spectra of 19 *(E)* shows a characteristic π–π* transition at 356 nm and a small band at 446 nm corresponding to n−π* transition (Fig. 2b). For 19 *(Z)*, the band of π−π* transition appears blueshifted to 316 nm, while the band at 446 nm (n−π* transition) is more noticeable. For all these compounds thermal $Z \rightarrow E$ isomerization is slow enough to allow the evaluation of *Z* isomer at the stabilized pss without evidence of decomposition. Between 17−24 hours in the dark, the recovery of the total percentage of the trans isomer (99 %), present in the initial pss, is observed, resulting in agreement with the UV–vis spectra as a function of time (See Supplementary data).

These experiments suggest that these derivatives could be used as optically controlled probes [22]. The photomodulation capacity of derivatives 8 and 19 and the percentages of photoisomerization were also evaluated through ^1H NMR (300 MHz) experiments. The experimental procedure consisted in placing the compounds previously dissolved in $CDCl_3$ in NMR tubes and then expose them to irradiation with UV light at λ=360 nm (8 W) for 90 min. Photoirradiated compounds spectra were recorded in the absence of light to minimize photoreversion during measurements. For both compounds, 90 % of the *Z* isomer was obtained, detecting the upfield shift of both aromatic and -CH_2O- signals (Fig. 2c) (Supplementary data).

2.4. *In vitro inhibition studies on AChE of the Z isomers*

Once tested photoisomerization ability, AChE inhibitory activity of 7–11 (*Z*), 17 (*Z*) and 19 (*Z*) was evaluated in vitro by Ellman's spectrophotometric method (for procedure see Quantitative AChE inhibition assay (isomer *Z*). Results are summarized in Table 3. Compounds 7 (*Z*), 9 (*Z*) and 19 (*Z*) showed IC_{50} values for AChE inhibition of 4.02, 0.85 y 0.43 μM, respectively, displaying a more powerful *in vitro* enzymatic response than its *E* isomer. In opposite, the *Z* isomer of 8 and 17 (both derivatives with odd linkers) showed less AChE inhibitory potency than the corresponding *E* isomer. We attribute this result to the odd number of carbons at the linker, based on our own previous experience with azobenzene compounds as amphiphiles, which observed difficulties in the synthesis and characterization only on analogs with odd number of carbons in the hydrocarbon fraction [23]. Even more, derivative 11 showed no activity in the *Z* configuration. Finally, this study indicated that the most powerful AChEI in the series is 19 (*Z*), with $IC_{50} = 0.43$ μM.

2.5. *Molecular modelling study*

Compound 19 (*Z*), the most active of the azo-derivatives synthesized, was chosen to shed light on their mode of action from a molecular insight perspective. Also, compound 17 (*Z*) and 19 (*E*) were modelled with the aim to study the role of the chain length and the azo group stereochemistry, respectively. Molecular docking and subsequent 100 ns molecular dynamics of the three systems (19 *(Z)*-AChE; 17 *(Z)*-AChE and 19 *(E)*-AChE) were performed. The three compounds are placed at the PAS of the enzyme and have part of one of the N-alkylpiperidinium moiety at the entrance of the main door (appointed as *outer* chain) (See Supplementary data).

The results clearly reveal that 19 (*Z*) is the only compound able to adopt a folded conformation that permits both piperidinium groups interact with the ASP72, simultaneously (outer piperidinium: 49 % occupancy, 1,8 Å; 162° and inner piperidinium: 92 % occupancy, 1,8 Å; 162°; Fig. 3a). Also, there is an additional hydrogen bond involving the azo group and backbone NH group of ARG289 or PHE288 (84 % occupancy, 2,2 Å; ≈156°). Hydrophobic interactions involve the aromatic surround of the PAS but no π-stacking interactions are observed since the distances and angles are not the proper ones. On the other hand, 19 (*E*) adopts a very different pose because of the planar geometry of the azo

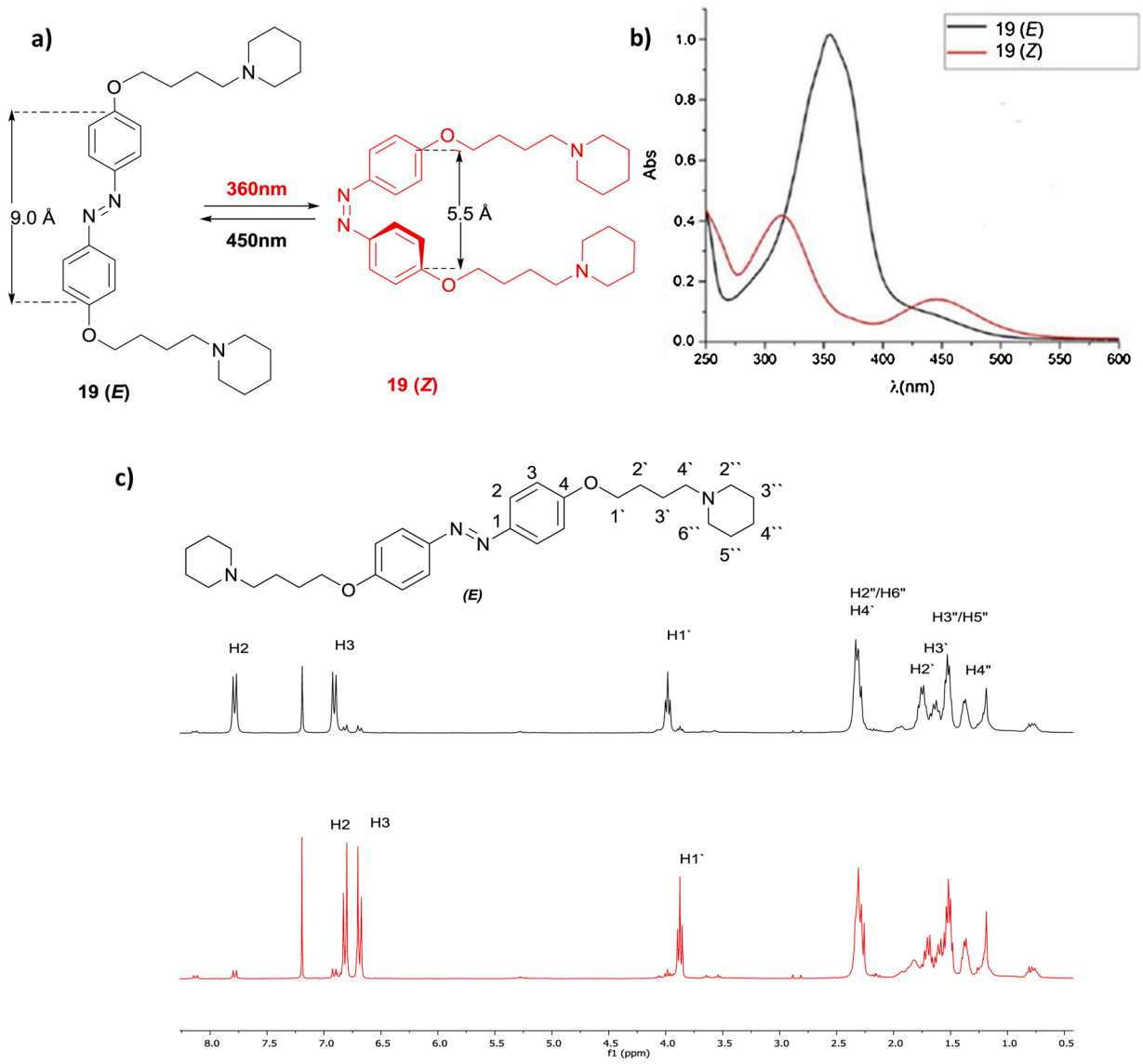

Fig. 2. (a) Photoisomerization of 19. (b) UV – Vis spectra of 19 before (–) and after (–) UV-light illumination (360 nm, 8 W, 5 min) in methanol (43 μM). (c) ^{1}H NMR of 19. Black: after irradiating with UV light (360 nm, 8 W, 5 min), showing the presence of 10 % of the *Z* isomer, assigning 19 (*E*). Red: after irradiating with UV light for 90 min, assigning the signals of H2, H3 and H1` of 19 (*Z*) with upfield shift of the signals, with respect to the (*E*) isomer.

Table 1
Inhibition of acetylcholinesterase activity for compounds 6-11 and 17-24.

	Compound	-NR_2	n	IC_{50} (μM)	log IC_{50} ± DS
Monosubstituted	6	piperidine	4	8.52	0.931 ± 0.086
	7	piperidine	6	5.16	0.713 ± 0.051
	8	piperidine	7	0.96	−0.018 ± 0.120
	9	piperidine	8	1.89	0.276 ± 0.104
	10	pyrrolidine	7	4.40	0.649 ± 0.070
	11	piperazine	7	>50	–
Disubstituted	17	piperidine	3	1.27	0.103 ± 0.046
	18	pyrrolidine	3	2.49	2.491 ± 0.098
	19	piperidine	4	0.84	−0.078 ± 0.093
	20	pyrrolidine	4	1.08	0.037 ± 0.030
	21	piperidine	5	0.65	−0.190 ± 0.054
	22	pyrrolidine	5	0.97	−0.015 ± 0.025
	23	piperidine	6	1.26	0.099 ± 0.044
	24	pyrrolidine	6	1.60	0.205 ± 0.059
	tacrine			0.029	−1.53 ± 0.050

Table 2
Comparison of the λmax. of the π–π * and n–π * transitions before and after photoisomerization of compounds 7, 9, 17, 19, indicating the photoconversion ratio.

Compound	Isomer *(E)* $\lambda_{máx.}$ (π–π*)	Isomer *(Z)* $\lambda_{máx}$ (π–π*); $\lambda_{máx.}$ (n–π*)	Photoconversion ratio (*E*: *Z*)
7	344 nm	314 nm; 435 nm	19:81
9	344 nm	314 nm; 438 nm	16:84
17	353 nm	314 nm; 446 nm	11:89
19	356 nm	316 nm; 446 nm	9:91

group [24]. As a result of this, compound 19 (*E*) is fully extended during the simulation time. Only an electrostatic interaction between the inner piperidinium and ASP72 is observed during a short time (~10 % occupancy, 1,85 Å; ≈160°). Then, 19 (*E*) can penetrate AChE deeper than the *Z* isomers and it is stabilized by π-π interaction between the azobenzene moiety and TRP279, PHE330, TYR334 and/or PHE75 residues, as represented in Fig. 3b.

It should be mentioned that compound 17 (*Z*) fits inside the gorge in

Table 3
The AChE inhibitory activity of the *E* and *Z* isomers of derivatives 7-11, 17 and 19.

				Isomer *E*		Isomer *Z*	
	Compound	**-NR_2**	**n**	**IC_{50} (μM)**	**log IC_{50} ± DS**	**IC_{50} (μM)**	**log IC_{50} ± DS**
Disubstituted	7	piperidine	6	5.16	0.713 ± 0.051	4.02	0.604 ± 0.013
	8	piperidine	7	0.96	0.649 ± 0.070	2.30	0.361 ± 0.038
	9	piperidine	8	1.89	0.276 ± 0.104	0.85	−0.072 ± 0.019
	11	piperazine	7	>50	–	>50	–
	17	piperidine	3	1.27	0.103 ± 0.046	2.46	0.391 ± 0.146
	19	piperidine	4	0.84	−0.078 ± 0.093	0.43	−0.369 ± 0.053

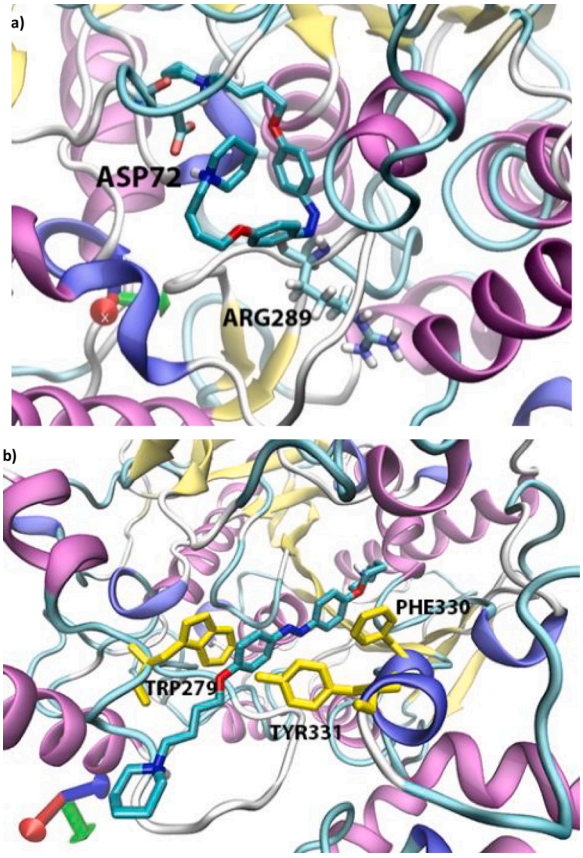

Fig. 3. a) Main polar interactions between inhibitor 19 (*Z*) and the enzyme acetylcholinesterase. b) π-stacking interactions between inhibitor 19 (*E*) and the aromatic residues (yellow) of the enzyme.

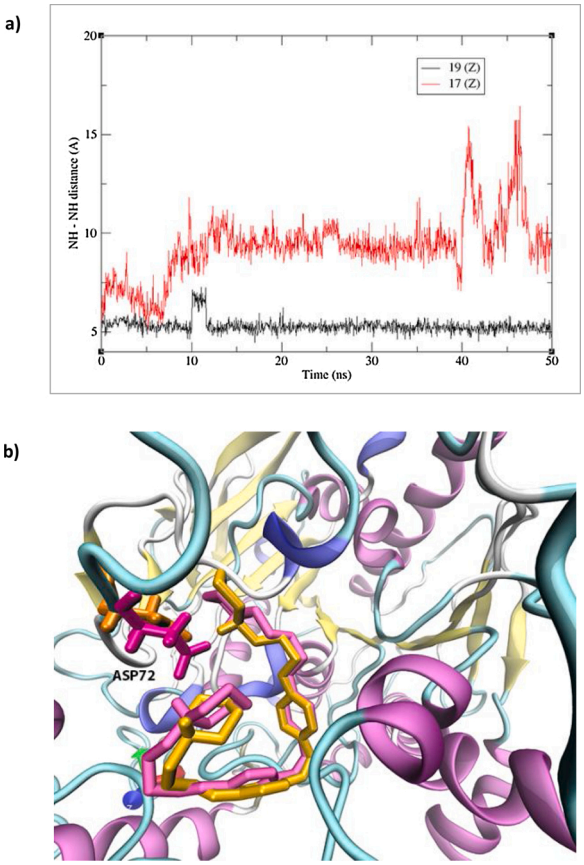

Fig. 4. a) Piperidinium NH^+–NH^+ distances of compounds 19 (*Z*) (black) and 17 (*Z*) (red) during the MD. b) Comparison of compounds 19 (*Z*) (pink) and 17 (*Z*) (orange) and ASP72 conformation at ~5 ns.

a similar fashion than 19 (*Z*) showing the same azo group interaction with backbone NH group of ARG289 or PHE288 (77 % occupancy; 2,3 Å; ≈160°). Even so, this compound is not able to achieve both electrostatic interactions with ASP72, simultaneously. Piperidinium NH+– NH + distances are represented for compounds 17 (*Z*) and 19 (*Z*) in Fig. 4a. While this distance is about 5,4 Å when both amines interact with ASP72 (system 19 (Z)-AChE), only during a short period of time both NH + groups of 17 (Z) are almost this nearest. Despite this, ASP72 conformation is not suitable for both electrostatic interactions (Fig. 4b).

This study allowed us to understand the conformation that 19 (*Z*) adopts inside AChE and the main interactions that rule the binding mode to the enzyme. This information could explain the higher affinity of this compound for AChE due to the two simultaneous electrostatic interactions as the stabilizing factor in the enzyme–inhibitor complex, not seen in the other two complexes. Also, this analysis evidenced not only the importance of the geometrical isomerism in these azo family, but the length chain requirement for best interactions. All this information will enable to suggest further structural modifications for the porpoise of designing new more effective AChEI.

Furthermore, the molecular modelling revealed that these compounds may also avoid the AChE interaction with amyloid-β since they are located at the PAS of the enzyme. This is important due to the evidence that AChE-Amyloid-β interaction promotes the A-β fibril formation, related to the most relevant neuropathological characteristic in AD, the senile plaques [25].

3. Conclusions

In conclusion, we have rationally designed and synthesized photochromic inhibitors of AChE, one of the most important enzymes involved in synaptic transmission. By microwave-assisted synthesis we obtained in high yields and short reaction times, new derivatives with a photomodulable azobenzene core monosubstituted at position 4 and disubstituted at 4 and 4′ positions with a hydrocarbon chain connected to a tertiary amine. All of these new compounds showed to be powerful *in vitro* AChE inhibitors and showed photoisomerization ability as long

with a slow thermal reversion. These results probe that these azo-compounds are efficient photoswitchable molecules with potential application in therapies based on synaptic communications. Compound 19 *(Z)* proved to be more effective AChEI (IC_{50} = 0.43 μM) than its *E* isomer, becoming the most active of the series. A molecular modelling study allowed us to propose that these inhibitors are located at the PAS of the enzyme. That means that, in addition to inhibit the enzymatic activity, these compounds can interfere in the β-amyloid pro-aggregating AChE-induced activity. It is to note that the molecular dynamic simulations allowed us to understand why the inhibitor 19 is more effective in its Z geometry. These studies suggest the importance in the rational design of the interaction optimization at the enzyme binding sites and demonstrate that azoderivatives reported here can be considered as promising candidate compounds for the development of new multifunctional drugs for the treatment of AD.

4. Experimental section

4.1. Quantitative AChE inhibition assay

AChE from electric eel (500 U) was purchased from Sigma (Buenos Aires, Argentina). The enzymatic inhibition was determined *in vitro* using the Ellman's spectrophotometric method with minor modifications [16,19]. Buffer phosphate A (8 mM K_2HPO_4, 2.3 mM NaH_2PO_4) was used to obtain 5 U/mL stock solution of the enzyme. Further dilution was carried out with buffer phosphate B (8 mM K_2HPO_4, 2.3 mM NaH_2PO_4, 0.15 M NaCl, 0.05 % Tween 20, pH 7.6) to produce 0.3 U/mL final enzyme solution. Substrate solution (0.6 mM ATCI) containing the Elman's reactive (0.5 mM DTNB) was prepared in 0.1 M Na_2HPO_4 solution (pH 7.5). Samples were dissolved in buffer phosphate B with 1.25 % $CHCl_3$ and 13.75 % of MeOH as a cosolvent mixture. Enzyme solution (300 μL) and sample solution (300 μL) were mixed in a test tube and incubated at r.t. (60 min). The reaction was started by adding the substrate solution (600 μL). The absorbance was recorded at 405 nm for 120 s at 25 °C on a JASCO V-630BIO (Tokyo, Japan) Spectrophotometer equipped with an EHCS-760 Peltier. Enzymatic activity was calculated by comparing the reaction rates between the sample and the blank. All reactions were performed in triplicate. The sample concentration reflecting 50 % inhibition (IC_{50}) was calculated by nonlinear regression of the response curve versus log (concentration), using GraphPadPrism 5. Tacrine was used as the reference inhibitor.

4.2. Quantitative AChE inhibition assay (isomer Z)

Inhibitory activity of the *Z* isomer was determined in the absence of light. Sample solution in MeOH (30 μL) was irradiated with UV light at 360 nm for 10 min. Then, 270 μL of buffer B and 300 μL of AChE solution were added and incubated 60 min avoiding the light. The whole process was performed in the dark to prevent $Z \rightarrow E$ isomerization. The test was continued as indicated in the previous point.

4.3. UV–vis spectroscopy

Switching experiments were done with an 8 W mercury arc lamp with filter of 360 nm from Pleuger Antwerp Brussels. The $Z \rightarrow E$ isomerization was accelerated by illumination with white light bulb of 60 W to evaluate photoreversion without decomposition. UV − vis spectroscopy data were measured with a Varian Cary 60 UV/Vis Spectrophotometer (Agilent, USA). Thermal $Z \rightarrow E$ isomerization was slow enough allowing the evaluation of all pss separately.

4.4. Molecular docking determinations

In order to prepare the ligands and the protein for the docking study, the geometry of compounds 17 (*E*), 19 (*Z*) and 19 (*E*) were optimized with semiempirical calculations (AM1) and the Hartree-Fock method (6−31 G (d, p) basis set) incorporated in the Gaussian 09 program [26–28]. Also the protein from the X-ray crystal structure of *Torpedo californica* AChE (PDB code 2ACE [29]) was prepared (i. e. hydrogen addition, charges calculation and atom types assignment). The program Autodock version 4.2.5.1 was chosen for the docking research using the implemented empirical free energy function [30]. The simulations were prepared, run and analyzed using the graphical interface program AutoDock Tools. A box including the active site, as well as the peripheral anionic site of the enzyme was defined as the simulation space. The auxiliary program Autogrid 4 was used for calculating the atomic interaction energy on a 0.375 Å grid between probes corresponding to each inhibitor atom type and the different protein atom types. All dihedrals in the compounds were able to rotate freely.

The Lamarckian genetic algorithm protocol was chosen for the docking performance and 256 independent simulations with a 150 members population size were run for each compound. Other parameters were set as default. After docking, the poses obtained were grouped according to all atom root-mean-square deviation (rmsd). The tolerance for each group is a RMSD of 2 Å position from the lowest-energy conformation. Then, a ranking was done with the clusters energy related to the lowest-energy conformer within each cluster.

4.5. Molecular dynamics simulations

MD simulations were performed starting from the Crystal structure of *Torpedo californica* acetylcholinesterase complexed with Xe, solved at 2.3 Å resolution (PDB entry: 3M3D [31]). The xenon atom was removed. The system was immersed in an octahedral box of TIP3P water molecules [32], the limits of which were at a minimum distance of 10 Å from the protein. Due to periodic boundary conditions, Ewald sums were used to treat long-range electrostatic interactions [33] for all systems. To maintain the covalent bonds between heavy atoms and hydrogen atoms, the SHAKE algorithm was used to maintain the geometric constraint of the bond during molecular dynamics simulations [34]. The integration of Newton's equations was performed to predict the atomic positions in a future time step of each atom of the protein, ligands, and water molecules, by the force fields parm99, gaff and TIP3P, respectively, all of them implemented in AMBER [35,36]. To regulate the temperature and pressure, the Berendsen thermostat and barostat were used throughout the simulation. The first step consisted of a short and gradual geometric optimization of all the atoms in the system in order to avoid that when starting the simulation, two or more atoms were too far from equilibrium position, which can cause undesired collisions. Subsequently, brief simulations of molecular dynamics were carried out using a 0.1 fs time step to increase gradually the kinetic energy of the atoms. To do this, the systems were slowly heated from 100 to 300 K, under constant volume conditions. The last step of the balancing step, to allow the systems to reach the proper density, consisted of a brief simulation at a constant temperature of 300 K using a 0.1 fs time step, under constant pressure of 1 bar. The atomic positions and velocities at the end of this equilibration step were taken as the starting point for the production of 100 ns MD simulations at 300 K temperature using a 2 fs time step.

Author statement

Brunella Biscussi was responsible for the data curation, formal analysis, investigation, methodology, visualization, writing original draft, review and editing; Maria Alejandra Sequeira for data curation, formal analysis, investigation, methodology, visualization, writing original draft; Victoria Richmond for the conceptualization, data curation, formal analysis, investigation, software, writing original draft; Pau Arroyo Mañez for the conceptualization, data curation, funding acquisition, investigation, software, supervision and writing original draft; Ana Paula Murray for the conceptualization, data curation, formal analysis, funding acquisition, investigation, methodology, project administration, resources, supervision, writing original draft, review

and editing.

Declaration of Competing Interest

The authors declare no conflict of interest.

Acknowledgements

This work was supported by CONICET (National Scientific and Technical Research Council), ANPCyT (National Agency for Promotion of Science and Technology) and UNS (Universidad Nacional del Sur).

Appendix A. Supplementary data

Supplementary material related to this article can be found, in the online version, at doi:https://doi.org/10.1016/j.jphotochem.2021.113375.

References

[1] S. Mazzitelli, F. Filipello, M. Rasile, E. Lauranzano, C. Starvaggi-Cucuzza, M. Tamborini, D. Pozzi, I. Barajon, T. Giorgino, A. Natalello, M. Matteoli, Amyloid-β 1-24 C-Terminal truncated fragment promotes Amyloid-β 1-42 aggregate formation in the healthy brain, Acta Neuropathol. Commun. 4 (1) (2016) 110, https://doi.org/10.1186/s40478-016-0381-9.

[2] G.D. Stanciu, A. Luca, R.N. Rusu, V. Bild, S.I. Beschea Chiriac, C. Solcan, W. Bild, D. C. Ababei, Alzheimer′s disease pharmacotherapy in relation to cholinergic system involvement, Biomolecules 10 (1) (2019) 1–20, https://doi.org/10.3390/biom10010040.

[3] Y. Huang, L. Mucke, Alzheimer mechanisms and therapeutic strategies, Cell 148 (6) (2012) 1204–1222, https://doi.org/10.1016/j.cell.2012.02.040.

[4] S.F. McHardy, H.Y.L. Wang, S.V. McCowen, M.C. Valdez, Recent advances in acetylcholinesterase inhibitors and reactivators: an update on the patent literature (2012-2015), Expert Opin. Ther. Pat. 27 (4) (2017) 455–476, https://doi.org/10.1080/13543776.2017.1272571.

[5] M.B. Colovic, D.Z. Krstic, T.D. Lazarevic-Pasti, A.M. Bondzic, V.M. Vasic, Acetylcholinesterase inhibitors: pharmacology and toxicology, Curr. Neuropharmacol. 11 (3) (2013) 315–335, https://doi.org/10.2174/1570159x11311030006.

[6] E.L. Konrath, C.D.S. Passos, L.C. Klein-Júnior, A.T. Henriques, Alkaloids as a source of potential anticholinesterase inhibitors for the treatment of alzheimer′s disease, J. Pharm. Pharmacol. 65 (12) (2013) 1701–1725, https://doi.org/10.1111/jphp.12090.

[7] J.L. Sussman, M. Harel, F. Frolow, C. Oefner, A. Goldman, L. Toker, I. Silman, Atomic structure of acetyicholinesterase from Torpedo calfornica: a prototypic acetyicholine-binding protein, Science (80-.) 253 (1991) 872–879.

[8] F. Pandolfi, D. De Vita, M. Bortolami, A. Coluccia, R. Di Santo, R. Costi, V. Andrisano, F. Alabiso, C. Bergamini, R. Fato, M. Bartolini, L. Scipione, New pyridine derivatives as inhibitors of acetylcholinesterase and amyloid aggregation, Eur. J. Med. Chem. 141 (2017) 197–210, https://doi.org/10.1016/j.ejmech.2017.09.022.

[9] A. Castro, A. Martinez, Peripheral and dual binding site acetylcholinesterase inhibitors: implications in treatment of alzheimers disease, Mini-Reviews Med. Chem. 1 (3) (2005) 267–272, https://doi.org/10.2174/1389557013406864.

[10] B. Reisinger, N. Kuzmanovic, P. Löffler, R. Merkl, B. König, R. Sterner, Exploiting protein symmetry to design light-controllable enzyme inhibitors, Angew. Chemie Int. Ed. 53 (2) (2014) 595–598, https://doi.org/10.1002/anie.201307207.

[11] J. Broichhagen, J.A. Frank, D. Trauner, A roadmap to success in Photopharmacology, Acc. Chem. Res. 48 (7) (2015) 1947–1960, https://doi.org/10.1021/acs.accounts.5b00129.

[12] J. Broichhagen, I. Jurastow, K. Iwan, W. Kummer, D. Trauner, Optical control of acetylcholinesterase with a tacrine switch, Angew. Chemie Int. Ed. 53 (29) (2014) 7657–7660, https://doi.org/10.1002/anie.201403666.

[13] M. Decker, Design of Hybrid Molecules for Drug Development, Elsevier Inc., 2017.

[14] J. Morstein, M. Awale, J.L. Reymond, D. Trauner, Mapping the azolog space enables the optical control of new biological targets, ACS Cent. Sci. 5 (4) (2019) 607–618, https://doi.org/10.1021/acscentsci.8b00881.

[15] M. Schoenberger, A. Damijonaitis, Z. Zhang, D. Nagel, D. Trauner, Development of a new photochromic ion channel blocker via Azologization of Fomocaine, ACS Chem. Neurosci. 5 (7) (2014) 514–518, https://doi.org/10.1021/cn500070w.

[16] B. Biscussi, V. Richmond, C.J. Baier, P. Arroyo Mañez, A.P. Murray, Design and microwave-assisted synthesis of aza-resveratrol analogues with potent cholinesterase inhibition, CNS Neurol. Disord. Drug Targets (2019).

[17] W. Wei, T. Tomohiro, M. Kodaka, H. Okuno, Selective Synthesis and Kinetic Measurement of 1 : 1 and 2 : 2 Cyclic Azobenzene Units. Society, 2000, pp. 8979–8987. No. 5.

[18] W. Szymański, J.M. Beierle, H.A.V. Kistemaker, W.A. Velema, B.L. Feringa, Reversible photocontrol of biological systems by the incorporation of molecular photoswitches, Chem. Rev. 113 (8) (2013) 6114–6178, https://doi.org/10.1021/cr300179f.

[19] G.L. Ellman, K.D. Courtney, V. Andres, R.M. Featherstone, A new and rapid colorimetric determination of acetylcholinesterase activity, Biochem. Pharmacol. 7 (2) (1961) 88–95, https://doi.org/10.1016/0006-2952(61)90145-9.

[20] R.S. Li, X.B. Wang, X.J. Hu, L.Y. Kong, Design, synthesis and evaluation of flavonoid derivatives as potential multifunctional acetylcholinesterase inhibitors against alzheimer′s disease, Bioorg. Med. Chem. Lett. 23 (9) (2013) 2636–2641, https://doi.org/10.1016/j.bmcl.2013.02.095.

[21] N.P. Alza, V. Richmond, C.J. Baier, E. Freire, R. Baggio, A.P. Murray, Synthesis and cholinesterase inhibition of cativic acid derivatives, Bioorg. Med. Chem. 22 (15) (2014) 3838–3849, https://doi.org/10.1016/j.bmc.2014.06.030.

[22] L.A. Benedini, M.A. Sequeira, M.L. Fanani, B. Maggio, V.I. Dodero, Development of a nonionic azobenzene amphiphile for remote photocontrol of a model biomembrane, J. Phys. Chem. B 120 (17) (2016) 4053–4063, https://doi.org/10.1021/acs.jpcb.6b00303.

[23] M.A. Sequeira, M.G. Herrera, Z.B. Quirolo, V.I. Dodero, Easy directed assembly of only nonionic azoamphiphile builds up functional azovesicles, RSC Adv. 6 (109) (2016) 108132–108135, https://doi.org/10.1039/c6ra20933e.

[24] G.S. Kumar, D.C. Neckers, Photochemistry of azobenzene-containing polymers, Chem. Rev. 89 (8) (1989) 1915–1925, https://doi.org/10.1021/cr00098a012.

[25] M. Bartolini, C. Bertucci, V. Cavrini, V. Andrisano, B -Amyloid aggregation induced by human acetylcholinesterase : inhibition studies, Biochem. Pharmacol. 65 (2003) 407–416.

[26] M.J.S. Dewar, E.G. Zoebisch, E.F. Healy, J.J.P. Stewart, Development and use of quantum mechanical molecular models. 76. AM1: a new general purpose quantum mechanical molecular model, J. Am. Chem. Soc. 107 (13) (1985) 3902–3909, https://doi.org/10.1021/ja00299a024.

[27] C.C.J. Roothaan, New developments in molecular orbital theory, Rev. Mod. Phys. 23 (2) (1951) 69–89, https://doi.org/10.1103/RevModPhys.23.69.

[28] Frisch M.J., Trucks G.W., S. H. et al. Gaussian 09.

[29] M.L. Raves, M. Harel, Y.-P. Pang, I. Silman, A. Kozikowski, J.L. Sussman, Structure of acetylcholinesterase complexed with the nootropic alkaloid, (-)-Huperzine a, Nat. Struct. Biol. 4 (1997) 57–63, https://doi.org/8989325.

[30] Auto-Dock 4.2 The Scripps Research Institute. Department of Molecular Biology, MB-5: La Jolla; CA 2013.

[31] J. Behnen, B. Brumshtein, L. Toker, I. Silman, J.L. Sussman, G. Klebe, A. Heine, 3M3D XRay, . (2009), https://doi.org/10.2210/pdb3M3D/pdb.

[32] W.L. Jorgensen, J. Chandrasekhar, J.D. Madura, R.W. Impey, M.L. Klein, Comparison of simple potential functions for simulating liquid water, J. Chem. Phys. 79 (2) (1983) 926–935, https://doi.org/10.1063/1.445869.

[33] B. Luty, I. Tironi, W. Van Gunsteren, Lattice-sum methods for calculating electrostatic interactions in molecular simulations, J. Chem. Phys. 103 (1995) 3014–3021.

[34] J.-P. Ryckaert, G. Ciccotti, H. Berendsen, Numerical integration of the cartesian equations of motion of a system with constraints: molecular dynamics of n-Alkanes, J. Comput. Phys. 23 (1977) 327–341.

[35] D. Pearlman, D. Case, J. Caldwell, W. Ross, T.E. Cheatham, S. Debolt, D. Ferguson, G. Seibel, P. Kollman, AMBER, a package of computer programs for applying molecular mechanics, normal mode analysis, molecular dynamics and free energy calculations to simulate the structural and energetic properties of molecules, Comput. Phys. Commun. 91 (1995) 1–41.

[36] V. Hornak, R. Abel, A. Okur, B. Strockbine, A. Roitberg, C. Simmerling, Comparison of multiple amber force fields and development of improved protein backbone parameters, Proteins 65 (2006) 712–725.